Journal of Alloys and Compounds 509 (2011) 6489–6496

Contents lists available at ScienceDirect

Journal of Alloys and Compounds

journal homepage: www.elsevier.com/locate/jallcom

# Production of Al nanocomposite reinforced by Fe–Al intermetallic, $Al_4C_3$ and nano-$Al_2O_3$ particles using wet milling in toluene

S.S. Razavi-Tousi [a,*], R. Yazdani-Rad [b], S.A. Manafi [a]

[a] Islamic Azad University, Shahrood Branch, Shahrood, Iran
[b] Materials and Energy Research Center, P.O. Box 31787/316, Karaj, Iran

ARTICLE INFO

*Article history:*
Received 28 August 2010
Received in revised form 2 December 2010
Accepted 18 March 2011
Available online 27 March 2011

*Keywords:*
Nanocomposite
Wet milling
Impurity
Dispersion
Sintering

ABSTRACT

Al matrix nanocomposites were produced by wet milling of Al and nano-alumina powders in a toluene media. X-ray diffraction patterns, inductively coupled plasma, carbon measurement analysis and scanning electron microscopy show that impurities introduced by decomposition of toluene and abrasion of balls and vials are uniformly dispersed in the Al matrix as $Al_4C_3$ and Fe–Al intermetallic particles. Though producing homogenous nanocomposites, these second phase particles seem to have a retarding effect on densification of nanocomposite powders.



## 1. Introduction

Mechanical alloying (MA) as a well known method for production of advanced materials usually suffers the problem of contaminations [1–3]. The contaminations usually are introduced by abrasion of balls and vial, or mechanochemical decomposition of process control agents (PCA).

Presence of contaminations is usually deemed as a detrimental phenomenon in various applications [4]. However it could be welcomed in some minor usages such as increasing thermal stability of nanocrystalline materials [5], accelerating synthesis of nanocrystalline materials [6], improvement of sintering properties [7], increasing electrocatalytic performance of alloy electrodes [8] and improving mechanical properties of some milled products [9–12].

Higher amounts of impurities may be expected in the case of wet milling of active metals such as aluminum, when collisions between vial, particles and balls take place in a hydrocarbonic media. However, there are several cases in which authors did not report any contamination caused by decomposition of toluene [13–15,6], hexane [16–18] or acetone [19] during mechanical milling of Al compounds.

On the other hand, there are cases indicating an effective presence of oxygen and carbon produced by mechanochemical decomposition of toluene or hexane during wet milling of Al [20–24]. This study focuses on production of Al nanocomposites reinforced by nano-alumina powder, as well as aluminum carbide and Fe–Al intermetallic inclusions introduced by decomposition of PCA and abrasion of balls and vials respectively.

## 2. Experimental

A high purity aluminum powder (Aldrich, no.: 518573, flakes, particle size: 1 mm) was separately mixed with 1, 3 and 7 vf% of MR70 alumina ($D_{50} \approx 500$ nm) and alumina nano-powder. Chemical composition of the as received Al powder was determined by inductively coupled plasma (ICP-AES-3410) analysis (Table 1). In order to calculate the mean particle size of nano-alumina powder, Brunauer–Emmett–Teller (BET) analysis was used to obtain surface area of nano-powder. Supposing mono sized spherical particles, a particle size of 39 nm was obtained for nano-alumina powder from Eq. (1):

$$d = \frac{6}{a_{s,BET} * \rho} \quad (1)$$

where $d$ is the particle size, $a_{s,BET}$ is the surface area obtained by BET analysis and $\rho$ is the density.

The mixtures were wet milled in a P5 planetary mill up to 22 h using stainless steel cup and balls in toluene media. The ball to powder ratio was 20:1 and the mill speed was maintained at 300 rpm. The produced powders were dried at 100 °C.

Chemical composition of each sample after milling was analyzed by ICP, and an ELTRA CS2000 carbon measurement instrument was used to quantify carbon impurity introduced by toluene. Each value obtained by carbon measurement instrument contains ±0.002 wt% error.

X-ray diffraction (XRD) patterns of powders were taken using a Philips (PW3710) X-ray diffractometer (30 kV and 25 mA) with Cu Kα radiation. Each peak was fitted on a pseudo-Voigt model [25], $K\alpha_2$ stripping was done through the

* Corresponding author.
*E-mail addresses:* ser105@mail.usask.ca, s.razavitousi@gmail.com (S.S. Razavi-Tousi).

0925-8388/$ – see front matter © 2011 Elsevier B.V. All rights reserved.
doi:10.1016/j.jallcom.2011.03.111

**Table 1**
Chemical composition of the as received Al powder obtained by ICP.

| Element | Ni | Cu | Zn | Mn | Fe | Cr | Zr | Mg | Si | Al |
|---|---|---|---|---|---|---|---|---|---|---|
| Weigh percent | <0.03 | 0.004 | 0.008 | 0.002 | <0.02 | <0.02 | 0.001 | <0.004 | 0.005 | Balance |

Rachinger method [26], afterward grain size of different samples was calculated by the Williamson–Hall method [27]:

$$B\cos\theta = \frac{0.9\lambda}{D} + 2\eta\sin\theta \quad (2)$$

where $B$, $\lambda$, $\theta$, $D$ and $\eta$ are full width at half maximum (FWHM), the wave length, peak position, crystallite size and lattice strain, respectively.

Particle size distribution of the powders was obtained using a Frisch Particle Sizer'analysette 22'.

In order to obtain bulk samples, the powders were pressed by an isostatic press in the air atmosphere (1 GPa), the green samples were sintered at 640 °C for 30, 60, 120, 240 and 480 min in the Ar atmosphere using a tube furnace.

The surface of sintered samples was examined using a Cambridge (Stereo Scan s360) scanning electron microscope (SEM). A Philips CM 200 FEG

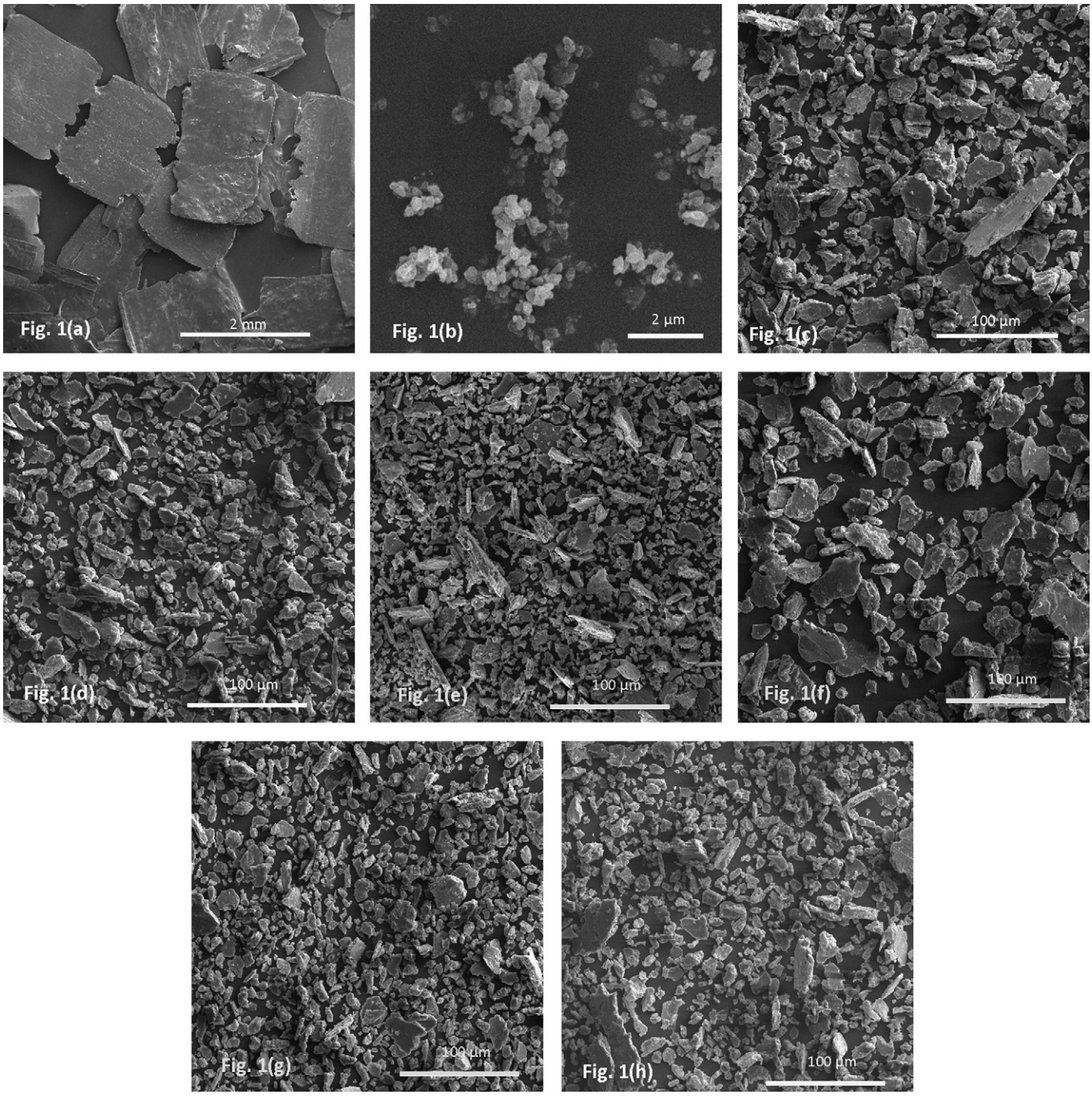


**Fig. 1.** SEM images of as received (a) Al and (b) submicron alumina powder. Morphology of (c) Al-1 vf% nano-alumina, (d) Al-3 vf% nano-alumina, e) Al-7 vf% nano-alumina, (f) Al-1 vf% submicron alumina, (g) Al-3 vf% submicron alumina and (h) Al-7 vf% submicron alumina powders milled for 22 h.

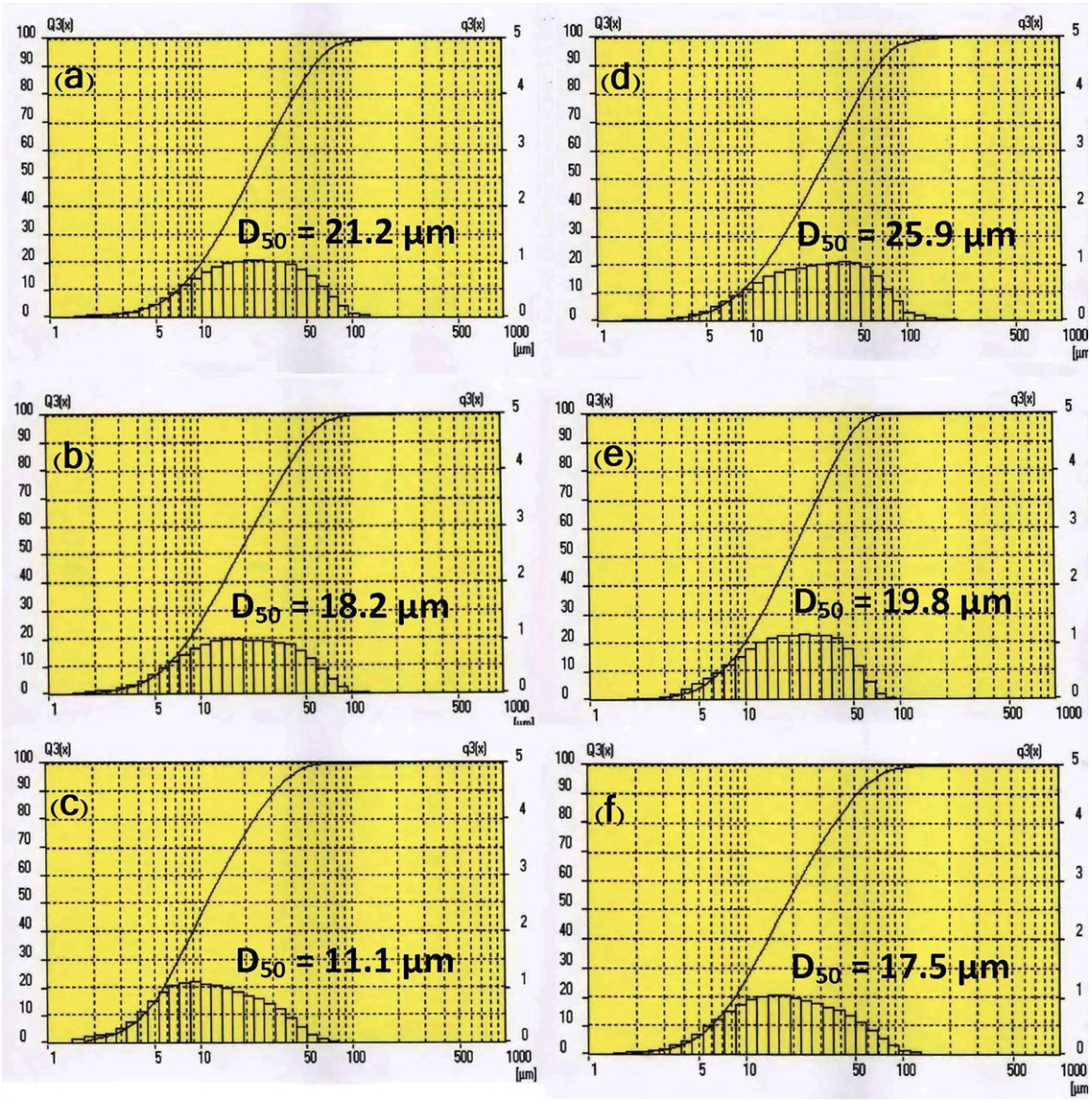


**Fig. 2.** Particle size distribution and $D_{50}$ of the composite powder after milling up to 22 h for samples reinforced by (a) 1 vf% nano-alumina, (b) 3 vf% nano-alumina, (c) 7 vf% nano-alumina, (d) 1 vf% submicron alumina, (e) 3 vf% submicron alumina and (f) 7 vf% submicron alumina powder.

transmission electron microscopy (TEM) was used to investigate samples microstructure.

## 3. Results and discussion

### 3.1. Powder synthesis

Fig. 1 shows SEM images of as received and milled powders. A marked decrease in particle size of Al powder after milling can be seen. Composite particles are shapeless and tend to smaller sizes as volume fraction of reinforcement phase increases. In order to study the effect of volume fraction and particle size of alumina phase on particle size of composite powders, accurate values of particle size were obtained by particle size analyzer. Fig. 2 shows the effect of volume fraction of alumina phase on particle size of the composite powders. It can be observed from the figure that greater volume fractions result in smaller particle sizes. However, the reduction in particle size is more prominent in composites with smaller reinforcing particle. The final particle size of milled powders depends on the equilibrium between fracture and cold welding mechanisms [1]. A ductile particle has a greater tendency toward cold welding rather than fracture, and there is a contrary trend for hard particles [28–30]. On the other hand, according to the Orowan theory [31], strength of particulate metal matrix composites increases as volume fraction of reinforcement phase increases or particle size of reinforcement phase decreases. Because higher volume fraction or smaller particle size of reinforcement phase result in harder composite particles, the tendency for fracture increases. Accordingly, the higher volume fraction or smaller particle size of alumina phase result in smaller particle size of composite powders.

Table 2 shows that considerable amounts of impurities are introduced during milling caused by abrasion of balls and vials. Though there is no trend for the effect of alumina phase on the amount of impurities introduced from stainless steel, the amount of carbon clearly depends on volume fraction of alumina phase. Fig. 3 shows that between 3.5 and 4.6 wt% carbon exists in the milled samples and the amount increases by volume fraction of the alumina phase.

Considering the effect of second phase particles on lattice of a ductile matrix during milling, one can understand the effect of alumina phase on the amount of carbon impurity. Toluene can be

**Table 2**
Chemical composition of the powder samples after milling obtained by ICP.

| | Ni | Cu | Zn | Mn | Fe | Cr | Zr | Mg | Si |
|---|---|---|---|---|---|---|---|---|---|
| 1 vf% nano-powder | 0.014 | 0.006 | 0.01 | 0.2 | 5.41 | 0.18 | <0.003 | 0.08 | <0.03 |
| 3 vf% nano-powder | <0.003 | 0.005 | 0.01 | 0.02 | 4.13 | <0.04 | <0.003 | <0.04 | <0.03 |
| 7 vf% nano-powder | 0.04 | 0.004 | 0.007 | 0.01 | 3.34 | <0.04 | <0.003 | <0.04 | <0.03 |
| 1 vf% submicron-powder | 0.01 | 0.004 | <0.007 | 0.01 | 2.69 | <0.04 | <0.003 | <0.04 | <0.03 |
| 3 vf% submicron-powder | 0.02 | 0.002 | 0.01 | 0.01 | 2.72 | <0.04 | <0.003 | <0.04 | <0.03 |
| 7 vf% submicron-powder | <0.003 | 0.003 | 0.01 | 0.01 | 2.51 | <0.04 | <0.003 | <0.04 | <0.03 |

decomposed by Al to produce hydrogen and aluminum carbide:

$$3C_6H_5CH_3 + 28Al = 7Al_4C_3 + 12H_2$$

Kinetic of the reaction depends on intensity of balls impact, the produced heat in collision zones and defects in Al lattice. The latter is affected by the amount of reinforcement phase; because of the additional deformation that soft particles must undergo during milling in the presence of hard non-deformable particles, there is a higher density of imperfections for a ductile matrix with a higher volume fraction of second phase particles [12].

As defects in Al lattice increases, there is a higher potential for reaction and consequently a more efficient progress in decomposition of toluene. Accordingly, higher amounts of alumina phase introduce more carbon to system.

The instability of Al lattice increases as the density of imperfections increases, thus a higher potential for reaction and consequently a more efficient progress in decomposition of toluene would be for higher amounts of alumina phase.

### 3.2. Sintered samples

XRD patterns of the samples sintered for 30, 120 and 480 min are typically presented in Fig. 4. After sintering for 30 min, small peaks of $Al_4C_3$ appear, and longer periods result in much noticeable peaks.

One can notice a slight sharpening in Al peaks as the sintering time is prolonged. In order to monitor the peak sharpening over time, FWHM of (1 1 1) reflection of Al is plotted for different samples. Fig. 5 shows that sintering time has a negligible effect on peak sharpening, thus one can conclude that microstructure of the Al matrix does not change very much during sintering, i.e. neither a considerable grain growth nor recovery take place during sintering.

Moreover, the result of Williamson–Hall equation for Al peaks confirms that grain size of sintered samples remained between

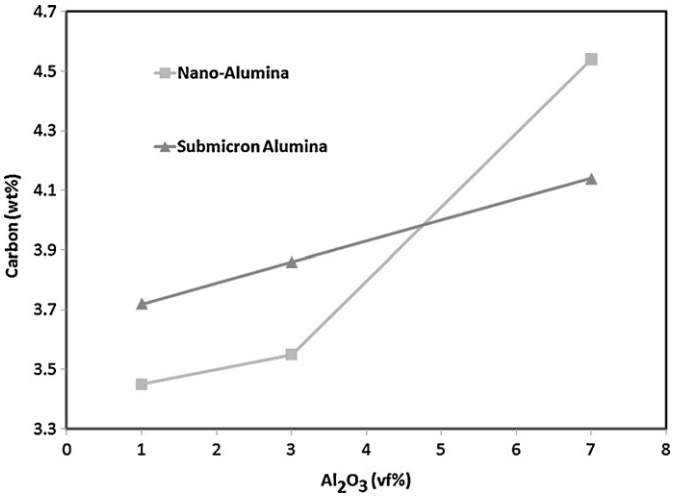


**Fig. 3.** Effect of volume fraction and particle size of alumina powder on carbon impurity introduced to the system from decomposition of toluene.

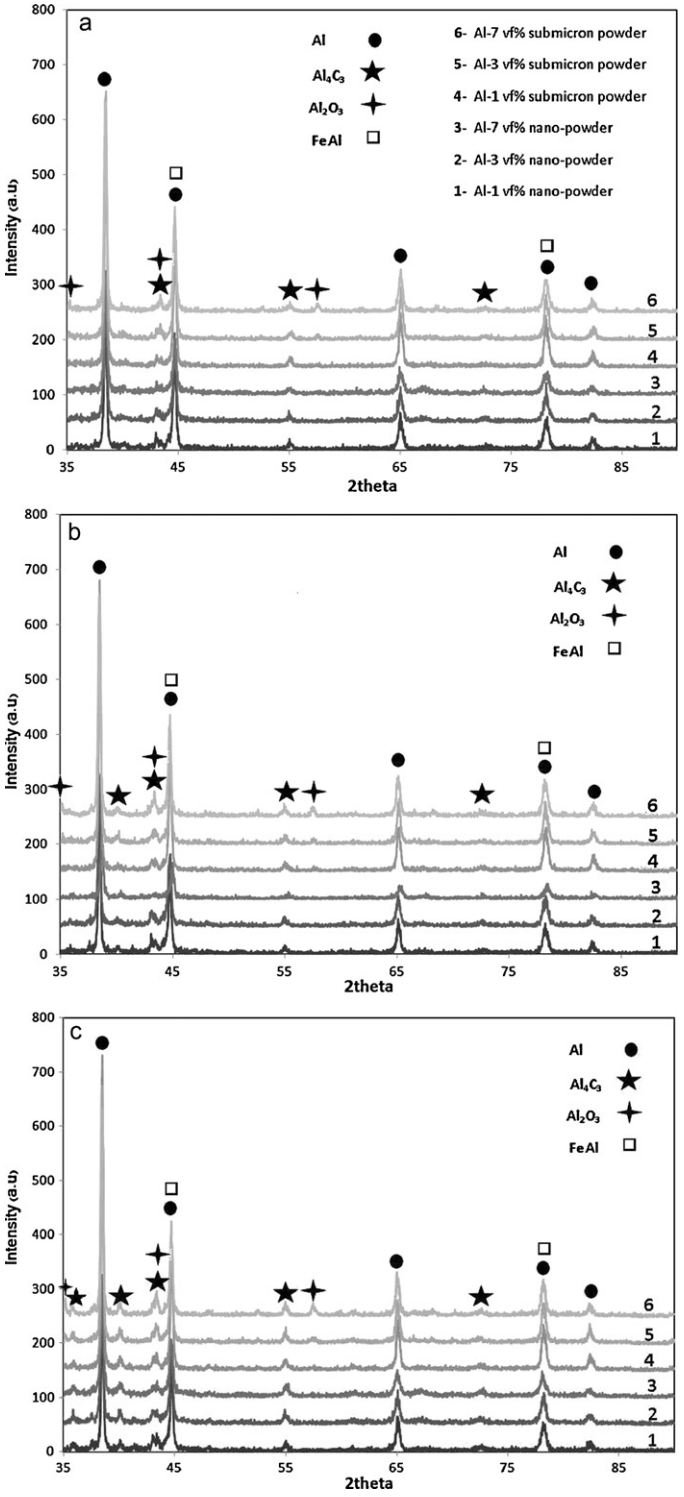


**Fig. 4.** XRD patterns of the samples sintered for (a) 30 min, (b) min 120 and (c) 480 min.

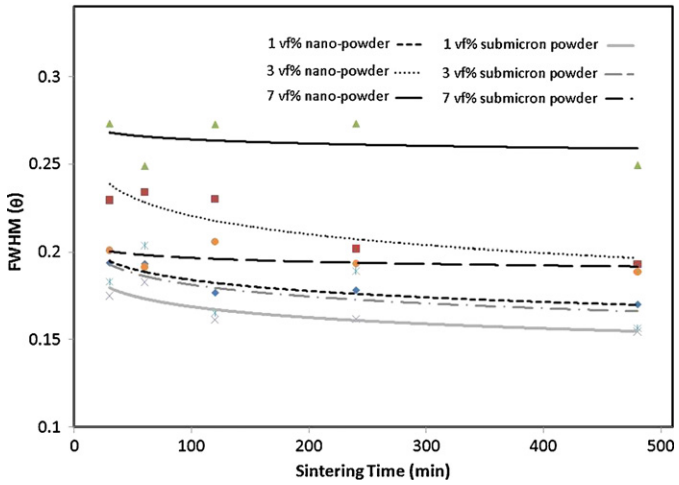


**Fig. 5.** Effect of sintering time on FWHM of (111) reflection of Al.

50 and 150 nm. As a typical sample, the Williamson–Hall plots of sintered Al-7 vf% submicron alumina are shown in Fig. 6.

The stagnation of grain growth is attributed to the Zener effect [32], results from the submicron and nano-alumina particles and the produced aluminum carbide inclusions. Similar results indicating stability of nanostructured metals at the presence of second phase particles can be found in the literature [33–37]. Moreover, in both nano and submicron reinforced composite powders, the grain boundary moves and the change in the neck area could also be delayed by the presence of alloying elements (Fe, Mg, Mn, ...) which could pin the boundary [38,39].

TEM images of Al reinforced by 3 vf% nano-alumina sintered for 120 min confirm the result of Williamson–Hall equation (Fig. 7). One can clearly notice the stability of nanostructured matrix of Al after sintering (Fig. 7(a)), and a uniform distribution of nano-alumina particles marked with arrows within the Al matrix (Fig. 7(b)).

As a typical sample, optical microscope (OM) and SEM images of polished surface of the Al sample reinforced by 7 vf% nano-alumina powder sintered for 120 min are presented in Fig. 8. OM images show that micrometric white particles are dispersed in the matrix (Fig. 8(a) and (b)). Back-scattered electron (BSE) images also show a uniform distribution of these white micrometric particles within

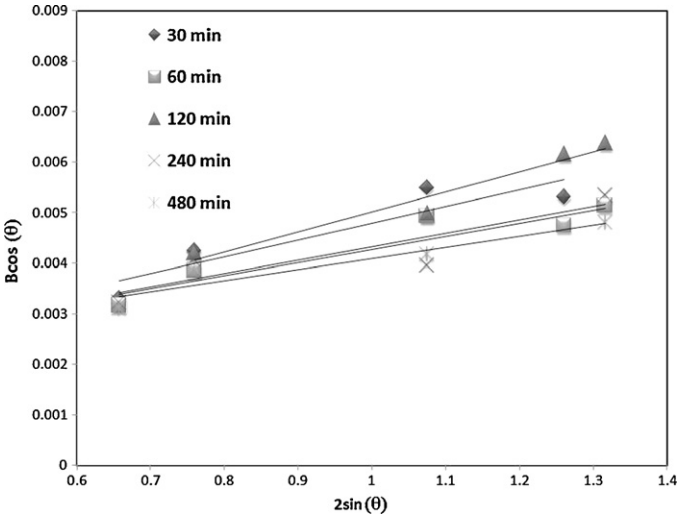


**Fig. 6.** Williamson-Hall plots of Al matrix reinforced by 7 vf% submicron alumina powder sintered for 30, 60, 120, 240 and 480 min.

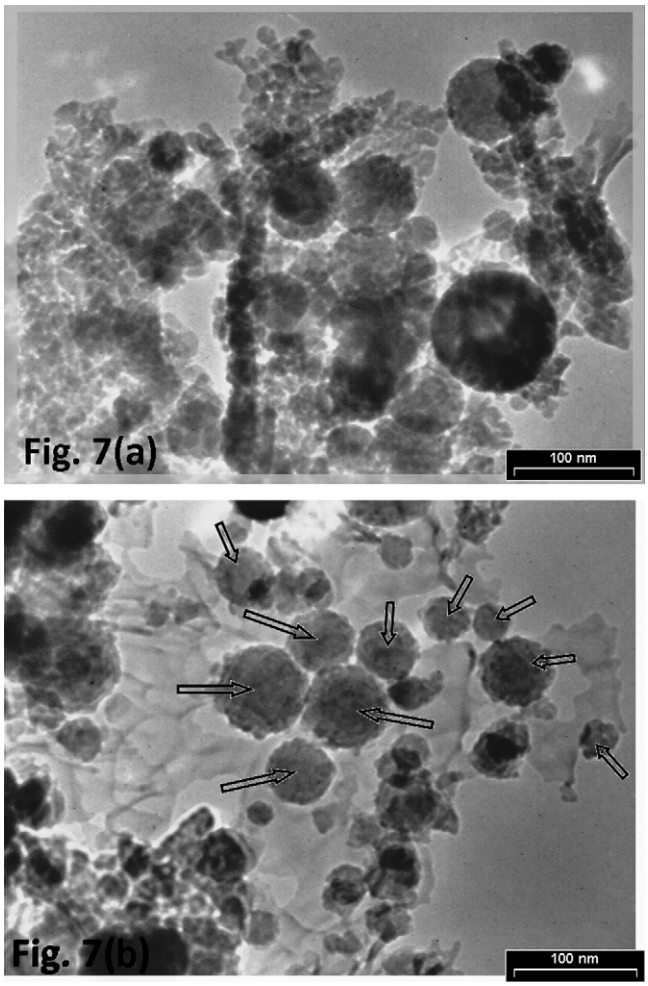


**Fig. 7.** Bright filed TEM images of Al reinforced by 3 vf% nano-alumina powder sintered for 120 min (a) the nanostructured matrix and (b) distribution of alumina particles (marked with arrows).

Al matrix (Fig. 8(c), (e) and (g)). Energy dispersive spectroscopy (EDS) indicates that there are Fe–Al intermetallic compounds, the white color is because of the presence of Fe element with a higher atomic weigh compared to Al (Fig. 8(h)). One should consider that the difference in color in BSE mode is due to phases with different chemical compositions, while secondary electron (SE) mode forms image due to the difference in topography. However, no marked sign of Fe–Al intermetallics peaks can be seen in the XRD patterns (Fig. 4), maybe due to the small portion of these phases or the overlap between peaks of FeAl as the most probable intermetallic phase and Al peaks.

There are also some fine particles that are visible in SE mode, as white tiny dots in Fig. 8(d) or submicron inclusions marked with arrows in Fig. 8(f), but no trace of them can be seen in BSE mode, which can be ascribed to $Al_4C_3$ particles. Absence of these fine particles in BSE mode should be due to the lower spatial resolution of BSE mode compared to SE mode. A similar microstructure can be seen for the Al sample reinforced by 3 vf% submicron alumina powder sintered for 240 min (Fig. 9). BSE image just depicts the distribution of Fe–Al intermetallic particles, but a higher magnified SE image shows a distribution of submicron particles, which can be attributed to $Al_2O_3$ or $Al_4C_3$ particles.

Fig. 8 clearly shows a poor densification in a way that almost all initial composite particles suffer absence of substantial neck formation/growth or coarsening mechanism. This is shown more clearly in Fig. 10; an incomplete densification can be seen for the Al sam-

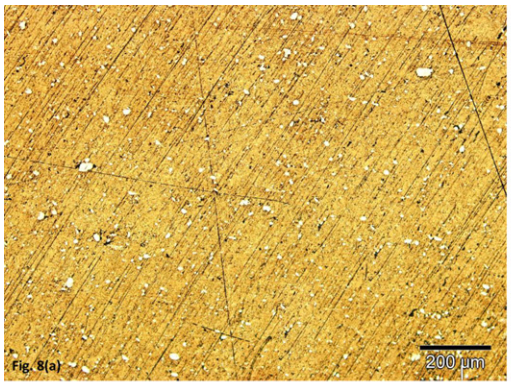


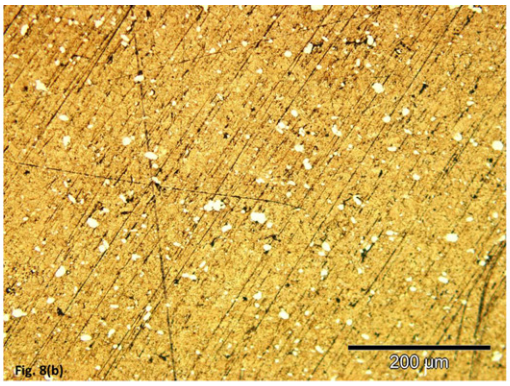


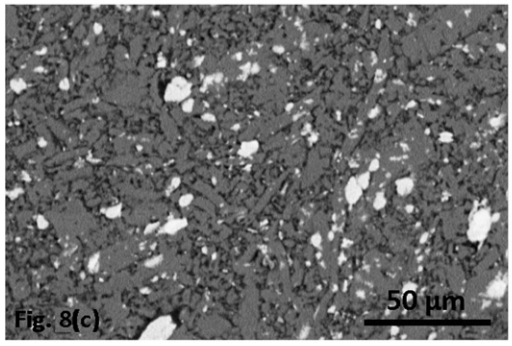


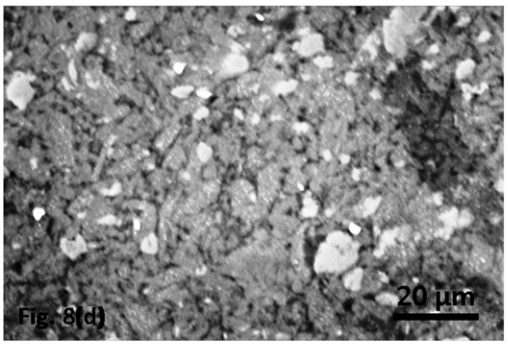


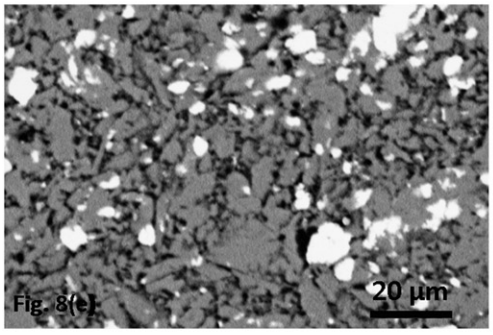


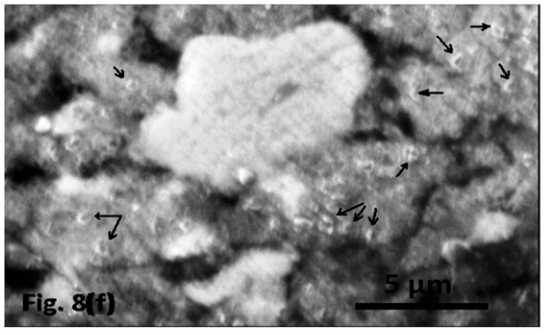


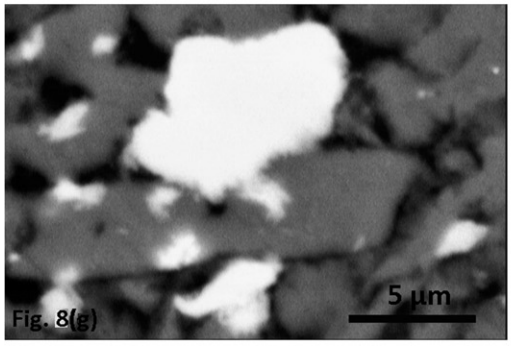


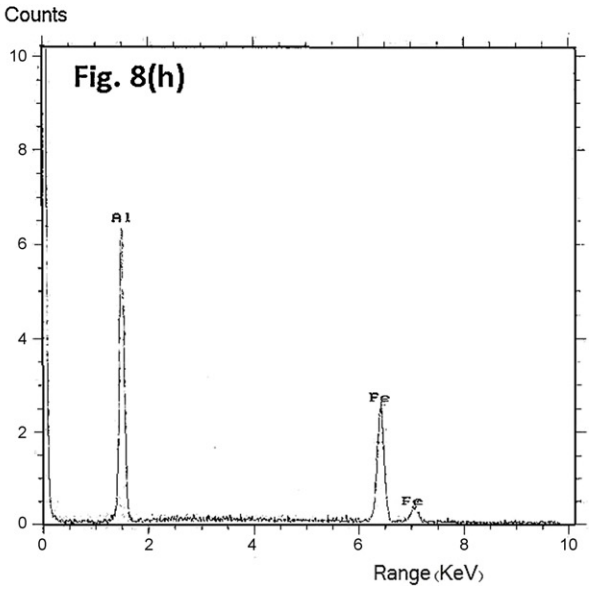


**Fig. 8.** OM and SEM images of the Al sample reinforced by 7 vf% nano-alumina powder sintered for 120 min (a) X 100 (OM), (b) X 200 (OM), (c) X 600 (BSE), (d) X 1000 (SE), (e) X 1000 (BSE), (f) X 6000 (SE), (g) X 6000 (BSE) and (h) EDS of a white particle.

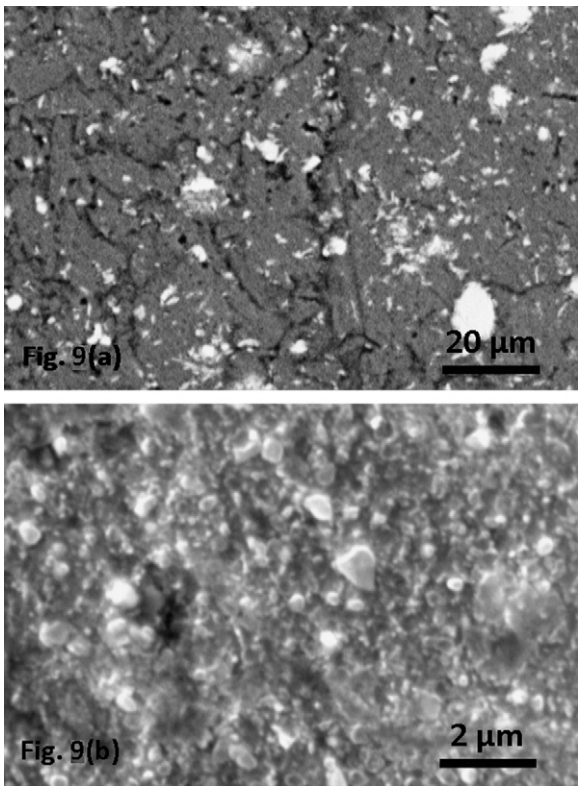


**Fig. 9.** SEM images of the Al sample reinforced by 3 vf% submicron alumina powder sintered for 240 min (a) X 1000 (BSE) and (b) X 10000 (SE).

ple reinforced by 7 vf% nano-alumina powder sintered for 60 min. Considering some necks marked with arrows and circles, one can simply realize that one or several retarding mechanisms prevent neck growth and coarsening.

In order to facilitate rationalization of densification behavior, sinterability of each sample was calculated using Eq. (3):

$$S = \frac{\rho_S - \rho_g}{\rho_T - \rho_g} \quad (3)$$

where $\rho_S$ is the sintered density, $\rho_g$ is the green density and $\rho_T$ is the theoretical density.

Fig. 11(a) shows that sintering durations more than 120 min has no effect on sinterability of the samples reinforced by nano-alumina powder, while it increases sluggishly for the samples reinforced by submicron alumina particles up to 480 min. Moreover, sinterability decreases markedly as the volume fraction of alumina phase increases.

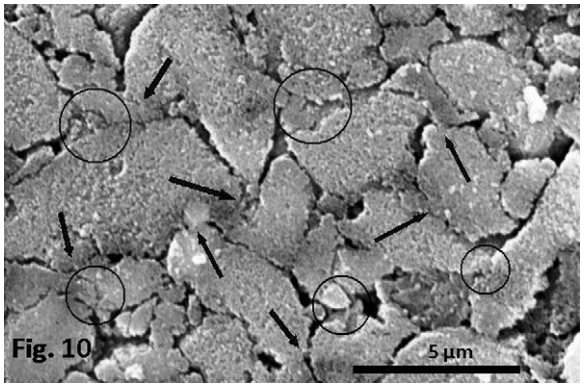


**Fig. 10.** SEM image (SE) of the Al sample reinforced by 7 vf% nano-alumina powder sintered for 60 min; arrows and circles mark the necks place.

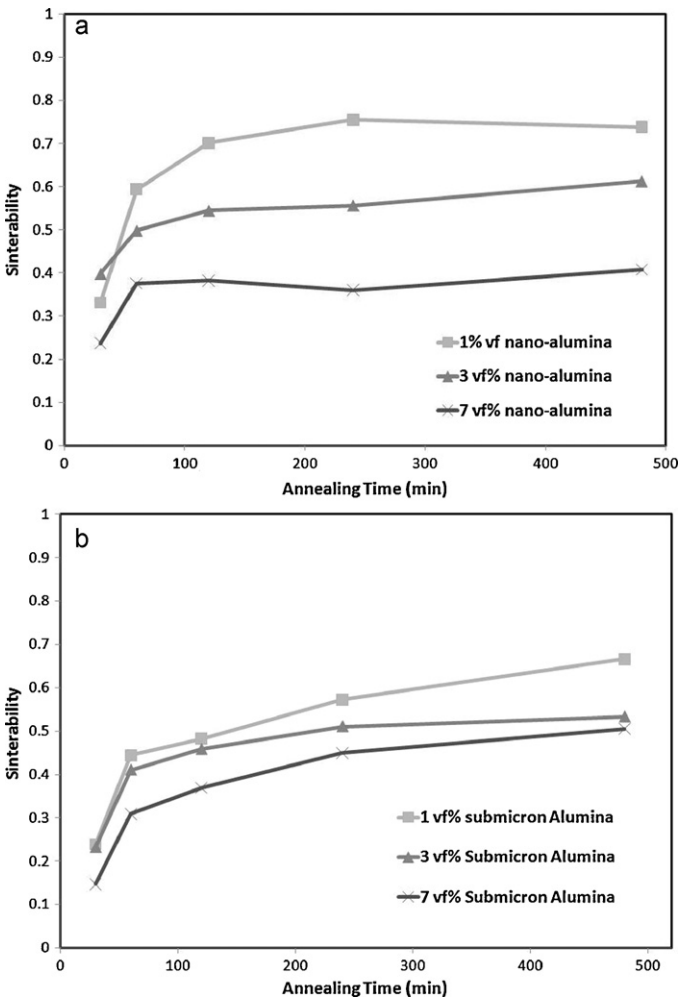


**Fig. 11.** Effect of sintering time on sinterability of Al nanocomposites (a) reinforced by nano-alumina and (b) reinforced by submicron alumina powder.

Remembering the limited grain growth of Al matrix during sintering, one can elucidate the poor densification and the trend observed in Fig. 11 according to the vital role of grain growth for densification. A very clear effect of grain growth on sintering was reported by Slamovich and Lange [40], approved by theoretical studies [41–43]. In order to reduce the free energy of system, formation of necks between the initial touching particles is thermodynamically feasible for any type of particles. Neck growth continues as long as the decrease in free energy due to a decrease in the external surface energy is more than the increase in free energy due to the increasing surface area of the boundary between particles. After that, densification proceeds by re-initiation of neck growth or coarsening (smaller particle to 'donate' its mass to the larger particle), both of them require grain boundary movement. Accordingly, the densification trend in Fig. 11 can be realized; the pinning force of alumina particles on Al grains decelerates neck growth or particle coarsening (Fig. 11(b)) or even stops them (Fig. 11(a)). The more inhibiting effect of the higher volume fractions is due to its effect on the pinning force estimated by Zener's theory [44].

Another retarding mechanism also should be considered; in an atomic scale point of view, the matter transfers between source and sinks during sintering in order to reduce the free energy of system [43]. Though have not an important influence on sinks, second phase particles cause the free surface of the metal containing them to become less effective as a source of matter because, as

the surface recedes, particles are exposed and a new, high energy interface is created [45]. Accordingly, the higher volume fraction of reinforcement phase, the smaller the inter-particle spacing and thus a more effective presence of alumina particles at surfaces will be, causing a negative effect on the sintering as can be seen in Fig. 11. This rationalization also can be used to explain the poor neck formation/growth and coarsening seen in Figs. 8 and 10.

## 4. Conclusion

Al matrix nanocomposite reinforced by $Al_2O_3$, $Al_4C_3$ and Fe–Al intermetallic particles were produced by wet milling in toluene media using stainless steel cup and balls. XRD patterns and carbon measurement confirmed the mechanochemical decomposition of toluene by Al. ICP analysis and SEM images showed presence of Fe impurity and distribution of Fe–Al intermetallic particles in the Al matrix. The nanostructured matrix of Al and a fine distribution of nano-alumina particles within matrix were affirmed by TEM images. Moreover, a poor densification progress was observed which is attributed to the inhibited grain growth due to the Zener mechanism as well as the effect of fine second phase particles on deactivation of sources from which matter transfers during sintering.

## Acknowledgement

The financial support received from the Materials and Energy Research Centre of Iran is acknowledged with gratitude.

## References

[1] C. Suryanarayana, Prog. Mater. Sci. 46 (2001) 1–184.
[2] C.C. Koch, Nanostruct. Mater. 9 (1997) 13–22.
[3] L. He, E. Ma, Mater. Sci. Eng. A 204 (1995) 240–245.
[4] M.S. El-Eskandarany, Mechanical Alloying for Fabrication of Advanced Engineering Materials, William Andrew Publishing, New York, 2000.
[5] R. Júarez, J.J. Sũnol, R. Berlanga, J. Bonastre, L. Escoda, J. Alloys Compd. 434–435 (2007) 472–476.
[6] J. Joardar, S.K. Pabi, B.S. Murty, J. Alloys Compd. 429 (2007) 204–210.
[7] C.B. Reid, J.S. Forrester, H.J. Goodshaw, E.H. Kisi, G.J. Suaning, Ceram. Int. 34 (2008) 1551–1556.
[8] M.A. Domínguez-Crespo, M. Plata-Torres, A.M. Torres-Huerta, I.A. Ortiz-Rodríguez, C. Ramírez-Rodríguez, E.M. Arce-Estrada, Mater. Charact. 56 (2006) 138–146.
[9] J.S. Benjamin, M.J. Bamford, Metal. Trans. A 8 (1977) 1301–1305.
[10] H. Kurishita, T. Kuwabara, M. Hasegawa, Mater. Sci. Eng. A 432 (2006) 245–252.
[11] S. Ohtsuka, S. Ukai, M. Fujiwara, T. Kaito, T. Narita, J. Phys. Chem. Solids 66 (2005) 571–575.
[12] S.S. Razavi Tousi, R. Yazdani Rad, E. Salahi, I. Mobasherpour, M. Razavi, Powder. Technol. 192 (2009) 346–351.
[13] D. Roy, D. Chakravarty, R. Mitra, I. Manna, J. Alloys Compd. 460 (2008) 320–325.
[14] D. Roy, R. Mitra, T. Chudoba, Z. Witczak, W. Lojkowski, H.-J. Fecht, I. Manna, Mater. Sci. Eng. A 497 (2008) 93–100.
[15] P. Nandi, P.P. Chattopadhyay, S.K. Pabi, I. Manna, Mater. Sci. Eng. A 359 (2003) 11–17.
[16] M. Nazarian Samani, A. Shokuhfar, A.R. Kamali, M. Hadi, J. Alloys Compd. 500 (2010) 30–33.
[17] F. Turquier, V.D. Cojocaru, M. Stir, R. Nicula, E. Burkel, J. Non-Cryst. Solids 353 (2007) 3417–3420.
[18] T.P. Yadav, N.K. Mukhopadhyay, R.S. Tiwari, O.N. Srivastava, Mater. Sci. Eng. A 393 (2005) 366–373.
[19] S.K. Vajpai, B.V. Mahesh, R.K. Dube, J. Alloys Compd. 476 (2009) 311–317.
[20] P.P. Choi, J.S. Kim, O.T.H. Nguyen, D.H. Kwon, Y.S. Kwon, J.C. Kim, Mater. Sci. Eng. A 449–451 (2007) 1119–1122.
[21] N.K. Mukhopadhyay, V. Kurup, V.C. Srivastava, P.B. Joshi, R.K. Mandal, J. Non-Cryst. Solids 334–335 (2004) 52–56.
[22] S. Mula, S. Ghosh, S.K. Pabi, Powder Technol. 191 (2009) 176–181.
[23] J.S. Kim, I.V. Povstugar, P.P. Choi, E.P. Yelsukov, Y.S. Kwon, J. Alloys Compd. 486 (2009) 511–514.
[24] J. Keskinen, A. Pogany, J. Rubin, P. Ruuskanen, Mater. Sci. Eng. A 196 (1995) 205–211.
[25] N. Aldea, A. Gluhoi, P. Marginean, C. Cosma, X. Yaning, Spectrochim. Acta B 55 (2000) 997–1008.
[26] W.A. Rachinger, J. Sci. Instrum. 25 (1948) 254–259.
[27] G.K. Williamson, W.H. Hall, Acta Metall. 1 (1953) 22–31.
[28] J.B. Fogognolo, F. Velasco, M.H. Robert, J.M. Torralba, Mater. Sci. Eng. A 342 (2003) 131–143.
[29] Z. Razavi Hesabi, A. Simchi, S.M. Seyed Reihani, Mater. Sci. Eng. A 428 (2006) 159–168.
[30] S.S. RazaviTousi, R. YazdaniRad, E. Salahi, I. Mobasherpour, M. Razavi, Powder Technol. 192 (2009) 346–351.
[31] E. Orowan, Symposium on Internal Stresses in Metals and Alloys, Institute of Metals, London, 1948, p. 451.
[32] S.S. RazaviTousi, M.B. Rahaei, M.S. Abdi, S.K. Sadrnezhaad, Ceram. Int. 36 (2010) 793–796.
[33] V.Y. Novikov, Mater. Lett. 62 (2008) 3748–3750.
[34] S.C. Tjong, H. Chen, Mater. Sci. Eng. R 45 (2004) 1–88.
[35] J.H. Driver, Scripta Mater. 51 (2004) 819–823.
[36] H. Cao, J.Y. Min, S.D. Wu, A.P. Xian, J.K. Shang, Mater. Sci. Eng. A 431 (2006) 86–91.
[37] T.S. Chou, Mater. Sci. Eng. A 223 (1997) 78–90.
[38] F. Liu, R. Kirchheim, Acta Mater. 51 (2004) 521–525.
[39] R. Kirchheim, Acta Mater. 50 (2002) 413–419.
[40] E.B. Slamovich, F.F. Lange, J. Am. Ceram. Soc. 75 (1992) 2498–2508.
[41] F.F. Lange, B.J. Kellett, J. Am. Ceram. Soc. 72 (1989) 735–741.
[42] F.F. Lange, J. Eur. Ceram. Soc. 28 (2008) 1509–1516.
[43] S.-J.L. Kang, Sintering, Densification, Grain Growth, and Microstructure, Elsevier, Oxford, 2005.
[44] C.S. Smith, Metall. Trans. Soc. A.I.M.E. 175 (1948) 15.
[45] M.F. Ashby, S. Bahk, J. Bevk, D. Turnbull, Prog. Mater. Sci. 25 (1980) 1–34.